Thermal Effects of 5G Frequency EM Waves on Ocular Tissue

Burak Aricioglu and Abdullah Ferikoglu

Department of Electrical and Electronics Engineering
Sakarya University of Applied Sciences, Sakarya, 54187, Turkey
baricioglu@subu.edu.tr, af@subu.edu.tr

Abstract — This research article aims to investigate the thermal effects on human eye due to exposure of EM (electromagnetic) field at 5G frequencies. A secondary purpose of the article is to show that SPICE, one of the most commonly used tools in circuit analysis, can be used to solve complex EM and bioheat transfer problems. Both electric field and temperature distributions in human eye are simulated with transmission line modelling (TLM) method. Also, finite element method (FEM) calculations are carried out for comparison. Temperature distributions are calculated for 30 minutes of EM radiation exposure. As a subject of the simulation, a human is chosen that the power density of incoming field at the human eye is assumed as the maximum of the ICNIRP general public exposure limits. A good consistency between TLM and FEM based simulations is found. A new transmission line model based on Debye parametric model is generated for simulation of EM field distribution in the tissues. With this generated transmission line, the results for the frequencies of interest can be obtained via single simulation. Also, a new transmission line model is developed for the temperature distribution simulation in which the effects of noncompressible fluid flow such as non-unidirectional blood flow in tissues and flow in aqueous humor are taken into consideration.

Index Terms — 5G, bioheat transfer, electromagnetic field, TLM.

I. INTRODUCTION

Wireless communication technologies have been advancing to meet constantly changing demands or to overcome the challenges such as capacity, quality of service, data rate, cost etc. [1]. To facilitate such increasing demands a new mobile cellular network architecture, 5G (fifth generation), is needed since, they cannot be provided sufficiently by the 4G (fourth generation) technologies [2].

However, these advances in wireless communication technologies cause some public concerns about possible hazardous health effects of mobile communication. In the recent decades, concerns on EM (electromagnetic) power absorption by the human eye have been raised since as the wireless communication advances, the chance of direct EM radiation exposure of the eye in a GHz frequency band increases [3]. Naturally, the public looks for reassurance that they are not in any way harmful or dangerous environment.

In the literature, numerous studies have been conducted to investigate the electromagnetic power absorption in the human eye with different models as well as for different frequencies. In Table 1, some of the related studies in the literature are given in terms of their eye model, frequency of interest and EM wave and bioheat transfer solution method.

Table 1: Some of the studies on EM power absorption by the human eye in the literature

Study	Eye Tissue Content	Freq. (GHz)	EM Solution Method	Bioheat Solution Method
[3]	ah, c, i, l, s, vh	0.9−10	FDTD	FDM
[4]	c, h, l, s	6, 18, 30	FDTD	FEM
[5]	ah, c, l, s, vh	0.6−6	FDTD	FDTD
[6]	ah, c, i, l, pc, s, vh	0.9	FEM	FEM
[7]	ah, c, i, l, s, vh	0.9−10	FDTD	FDM
[8]	ah, c, i, l, pc, s, vh	0.9, 1.8	FEM	FEM
[9]	ah, c, l, s	0.6−6	FDTD	-
[10]	ah, c, l, s	0.6−4	FDTD	-
[11]	ah, c, ch, i, l, r, s, vh	0.915	FDTD	-
[12]	ah, c, ch, i, l, m, r, s, vh	0.9, 2.6, 28	FIT	-

*ah: aqueous humor, c: cornea, ch: choroid, i: iris, l: lens, m: muscle, pc: posterior chamber, r: retina, s: sclera, vh: vitreous humor, FDTD: finite difference time domain, FDM: finite difference method, FEM: finite element method, FIT: finite integration theory.

In this study, thermal effects of EM waves at 5G frequencies on the human eye is investigated. Both EM field distribution and bioheat transfer in the eye is solved with transmission line modelling (TLM) method. Also, they are solved with FEM for comparison. The TLM based simulations are carried out in NGSpice environment while the FEM based simulations are carried out in COMSOL Multiphysics environment.

TLM is used in the literature as a numerical solving method for some types of partial differential equations. These equations are wave equation that can be used to define EM propagation in lossless media, diffusion equation that can be used to define bioheat transfer and an equation that is linear combination of wave and diffusion equations which can be used to define EM propagation in lossy media. The main advantages of TLM are unconditional stability and non-requirement of matrix inversion for time-domain solutions [13].

The model of the eye is taken as described in [14]. It consists of six tissues: aqueous humor, cornea, iris, lens, sclera and vitreous humor as shown in Fig. 1.
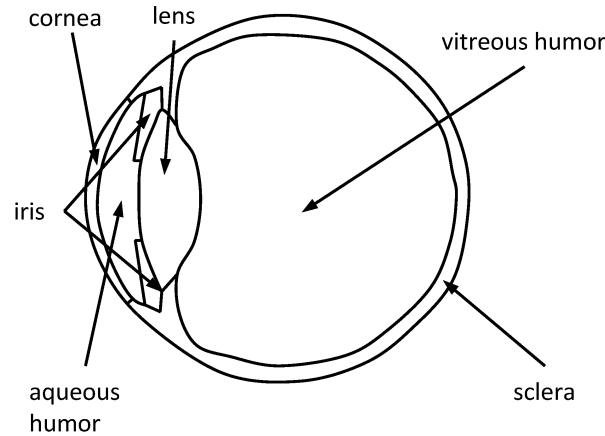

Fig. 1. 2D model of eye used in the study [14].

5G carrier frequencies considered in the study are 0.7GHz, 3.6GHz, 26GHz, 32GHz and 42GHz. According to European Conference of Postal and Telecommunications Administrations (CEPT) report:

- The Radio Spectrum Policy Group (RSPG) considers 0.7GHz band for indoor and nationwide 5G coverage.
- The RSPG considers 3.6GHz band to be the primary band for introducing 5G based services
- The RSPG recommends 26GHz band as a pioneer band.
- The RSPG considers 32GHz band as a promising band and 42GHz band as a viable option in the longer term [15].

The paper is so organized that, Section 2 provides materials and method, Section 3 contains simulations and results, and Section 4 offers the conclusion.

II. MATERIALS AND METHODS

Transmission line circuit theory can be applied to solve wave equations when $\lambda \gg l$ where λ is the wavelength and l is the spatial resolution [16]. Wavelength of an EM wave travelling through a lossy medium can be calculated as follows:

$$\lambda = \frac{c}{f\sqrt{\varepsilon_r \mu_r}}. \qquad (1)$$

Here c is the speed of light in vacuum, ε_r is the relative permittivity of the medium, μ_r is the relative permeability of the medium and f is the frequency.

The wavelengths of EM waves travelling through the tissues for the frequencies of interest are given in Table 2.

Table 2: Wavelengths (mm) of EM waves travelling through ocular tissues with respect to frequency

Tissue	0.7GHz	3.6GHz	26GHz	32GHz	42GHz
a	51.52	10.38	2.11	1.87	1.61
c	57.12	11.81	2.39	2.11	1.80
i	57.48	11.63	2.27	2.00	1.71
l	71.13	14.55	3.02	2.66	2.27
s	57.32	11.67	2.35	2.08	1.78
v	51.63	10.16	2.07	1.88	1.68

*a: aqueous humor, c: cornea, i: iris, l: lens, s: sclera, v: vitreous humor.

In literature, thermal wave models of bioheat transfer (TWMBT) is proposed for solving bioheat transfer problems [17-19]. The wavelength of thermal waves can be calculated as:

$$\lambda = \frac{2\sqrt{2}\pi}{\sqrt{(c_T/\alpha)^2 + \sqrt{(c_T/\alpha)^4 + 4(\omega_b C_b / k_T)^2}}}. \qquad (2)$$

Here c_T is the speed of thermal wave (m/s), α is the thermal diffusivity (m^2/s), ω_b is blood perfusion rate $(kg/m^3/s)$, C_b is specific heat capacity of blood $(Ws/kg/K)$ and k_T is thermal conductivity of tissue $(W/m/K)$. The speed of thermal wave and thermal diffusivity is defined as follow:

$$c_T = \sqrt{\frac{\alpha}{\tau}}, \alpha = \frac{k_T}{\rho_T C}. \qquad (3)$$

Here ρ_T is density of tissue (kg/m^3), C is specific heat capacity of tissue $(Ws/kg/K)$, and τ is thermal relaxation time of tissues (s).

There are several studies conducting on finding thermal relaxation time of tissues [20-23] and its value varies between 0.426 and 50 seconds. By examining (2) and (3) the thermal wavelength and thermal relaxation time are proportional. Thermal relaxation time selected as its lowest value to determine spatial resolution for solving bioheat transfer problem with TLM. For this value thermal wavelength values in the ocular tissues are given in Table 3.

The wavelength values given in Tables 2 and 3 is used to determine the 2D-TLM mesh size to ensure the spatial

resolution is much smaller than wavelengths ($l \ll \lambda$). The mesh size will be given in Section III.

Table 3: Wavelength (mm) of thermal waves travelling in ocular tissues

Aqueous Humor	Cornea	Iris	Lens	Sclera	Vitreous Humor
1.64	1.61	1.57	1.53	1.57	1.63

A. TLM for electromagnetic wave solution

The field equations for a plane wave in a medium can be analogous to the circuit equations for a wave on a transmission line. This similarity can be favourably used for the analysis of a travelling EM wave in a medium based on transmission line analogy.

It is assumed that the incoming EM wave is characterized by TM (transverse magnetic) fields (TM-mode) to simplify the problem as in [6, 8, 24, 25]. Moreover, TM or TE (transvers electric) mode cavity resonators are usually employed in the current mobile base stations [26,27] and they will be still useful for 5G base stations [28].

It is very well established in the literature that TM or TE mode EM wave problems can be solved with 2D-TLM method [29]. Hence, 2D-TLM shown in Fig. 2 can be used to solve TM mode EM wave problems.

Consider a TM wave propagating along z direction in a lossy medium. The only none zero field components are H_x, H_y and E_z. Using Maxwell's Equations, the following equations are obtained:

$$\frac{\partial E_z}{\partial x} = \mu \frac{\partial H_y}{\partial t}, \qquad (4)$$

$$\frac{\partial E_z}{\partial y} = -\mu \frac{\partial H_x}{\partial t}, \qquad (5)$$

$$\frac{\partial H_y}{\partial x} - \frac{\partial H_x}{\partial y} = \sigma E_z + \varepsilon \frac{\partial E_z}{\partial t}. \qquad (6)$$

By taking derivatives of (4) and (5) with respect to x and y respectively, combine the resultants with (6) yields to:

$$\frac{\partial^2 E_z}{\partial x^2} + \frac{\partial^2 E_z}{\partial y^2} = \mu \sigma \frac{\partial E_z}{\partial t} + \mu \varepsilon \frac{\partial^2 E_z}{\partial t^2}. \qquad (7)$$

For solving (7), the transmission line shown in Fig. 2 can be used. In the figure V is voltage, R, L, C and G are resistance, inductance, capacitance and conductance per meter of the transmission line respectively and Δl is the unit length of the transmission line in the both x and y axis. If KVL (Kirchhoff's voltage law) is applied along x and y axis the followings are obtained, respectively:

$$-\frac{\partial V}{\partial x} = RI_x + L\frac{\partial I_x}{\partial t}, \qquad (8)$$

$$-\frac{\partial V}{\partial y} = RI_y + L\frac{\partial I_y}{\partial t}. \qquad (9)$$

Then, if KCL (Kirchhoff's current law) is applied to the node V shown in Fig. 2:

$$\frac{\partial I_x}{\partial x} + \frac{\partial I_y}{\partial y} = -2GV - 2C\frac{\partial V}{\partial t}, \qquad (10)$$

is obtained. By taking derivatives of (8) and (9) with respect to x and y respectively and combine the resultants with (10) yields to:

$$\frac{\partial^2 V}{\partial x^2} + \frac{\partial^2 V}{\partial y^2} = 2RGV + 2RC\frac{\partial V}{\partial t} + 2LG\frac{\partial V}{\partial t} + 2LC\frac{\partial^2 V}{\partial t^2}. \qquad (11)$$

If the value of R is taken as negligibly small or zero below equivalence can be established between (7) and (11):

$$V \leftrightarrow E_z, \; I_x \leftrightarrow H_y, \; -I_y \leftrightarrow H_x,$$
$$L \leftrightarrow \mu, \; 2C \leftrightarrow \varepsilon, \; 2G \leftrightarrow \sigma. \qquad (12)$$

The electrical parameters of the tissues are given in Table 4 with respect to frequency.
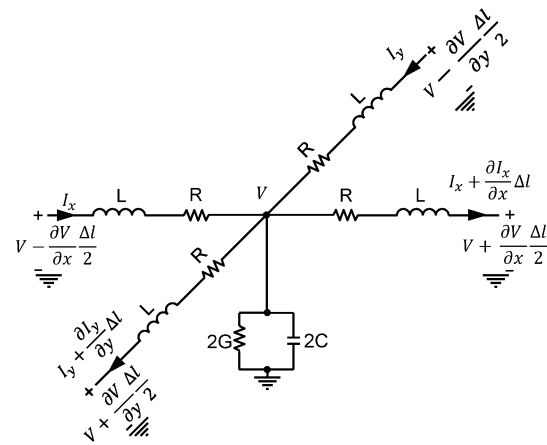

Fig. 2. 2D Lumped model of transmission line.

Table 4: Electrical parameters of ocular tissues with respect to frequency [30]

Tissue		0.7GHz	3.6GHz	26GHz	32GHz	42GHz
a	ε_r	69.20	64.40	30.0	25.1	19.7
	σ	2.34	4.69	41.4	48.0	56.3
c	ε_r	56.30	49.80	23.4	19.8	15.7
	σ	1.31	3.26	30.8	35.7	41.8
i	ε_r	55.60	51.30	25.8	22.0	17.5
	σ	0.88	2.65	31.6	37.2	44.4
l	ε_r	36.30	32.80	14.6	12.4	9.87
	σ	0.44	1.76	19.4	22.3	25.9
s	ε_r	55.9	51.0	24.1	20.4	16.1
	σ	1.1	3.0	31.4	36.5	42.9
v	ε_r	68.90	67.30	31.1	24.9	18.0
	σ	1.58	3.58	47.9	55.5	63.9

*a: aqueous humor, c: cornea, i: iris, l: lens, s: sclera, v: vitreous humor.

The value of μ_r (relative permeability) is selected as 1, since human tissues are a non-magnetic material that their magnetic permeability is same as or very close to that of vacuum [31,32].

In classical TLM method, it is not possible to solve a multi-frequency EM field distribution problem in a lossy media with a single simulation. Simulations must be carried as many as the number of the frequencies of interest. In this paper, a new transmission line model is design to make it possible to solve such multi-frequency EM field distribution problem with a single simulation.

In the literature, there are studies that employ parametric model of tissues' dielectric properties in order to solve a multi-frequency EM problem with a single simulation [33-35].

There are two parametric models of tissues commonly employed in the literature. These are Debye and Cole-Cole [36] parametric models. In both models, the dielectric properties of tissues can be expressed as a function of frequency over some frequency range. Debye parametric model is usually preferred because of its lower computational complexity and it can be easily expressed in time and frequency domain. On the other hand, Cole-Cole parametric model offers higher accuracy, and it can model the dielectric properties of tissues for a very large frequency range (typically from Hz to THz).

In this study, Debye parametric model is employed due to its lower computational complexity and it can be easily synthesized with an RC ladder network as it will be discussed in this section.

The Debye parametric model that describes the complex permittivity of a lossy medium is given in (13):

$$\varepsilon(\omega) = \varepsilon'(\omega) - j\varepsilon''(\omega) = \varepsilon_\infty + \frac{\sigma_s}{j\omega\varepsilon_0} + \sum_{i=1}^{n} \frac{\Delta\varepsilon_i}{1+j\omega\tau_i}. \quad (13)$$

Here $\varepsilon'(\omega)$ and $\varepsilon''(\omega)$ relative permittivity and dielectric loss factor respectively, n is the total number of Debye poles, ε_∞ is relative permittivity at the highest frequency (usually in THz region), σ_s the static ionic conductivity, ε_0 is the permittivity of free space, $\Delta\varepsilon_i$ is the change in the relative permittivity and τ_i is the ith relaxation constant at i^{th} dispersion.

The relation between conductivity of medium (σ) and dielectric loss factor $\varepsilon''(\omega)$ is given in (14):

$$\sigma = \omega\varepsilon_0\varepsilon''(\omega). \quad (14)$$

The parallel admittance per meter of the transmission line shown in Fig. 2 is given as:

$$Y(\omega) = 2(G + j\omega C). \quad (15)$$

Using (12) and (14), the parallel admittance can be described in terms of Debye parameters as given in (16):

$$Y(\omega) = 2(G + j\omega C),$$

$$2(G + j\omega C) \leftrightarrow \sigma + j\omega\varepsilon,$$

$$\sigma + j\omega\varepsilon \leftrightarrow j\omega\varepsilon_0(\varepsilon'(\omega) - j\varepsilon''(\omega)), \quad (16)$$

$$Y(\omega) \leftrightarrow j\omega\varepsilon_0(\varepsilon_\infty + \frac{\sigma_s}{j\omega\varepsilon_0} + \sum_{i=1}^{n} \frac{\Delta\varepsilon_i}{1+j\omega\tau_i}).$$

The parametric model of the parallel admittance $Y(\omega)$ given in (16) can be easily synthesized with Foster II circuit synthetization method as an RC ladder network.

The method is given in (17):

$$\frac{Y(\omega)}{j\omega} = Y_\infty + \frac{Y_0}{j\omega} + \sum_{i=1}^{n} \frac{K_i}{j\omega+\alpha_i}. \quad (17)$$

Where Y_∞ is the parallel capacitance, Y_0 is the parallel conductance and $\frac{K_i}{j\omega+\alpha_i}$ term is the pole introduced by a parallel admittance of a series RC branch. Using the relation given in (17) transmission line model of the tissues based on Debye parametric model can be generated as in Fig. 3. Here the number of Debye poles is three. Moreover, the relation between the synthesized parallel admittance and Debye parameters are given in Table 5.
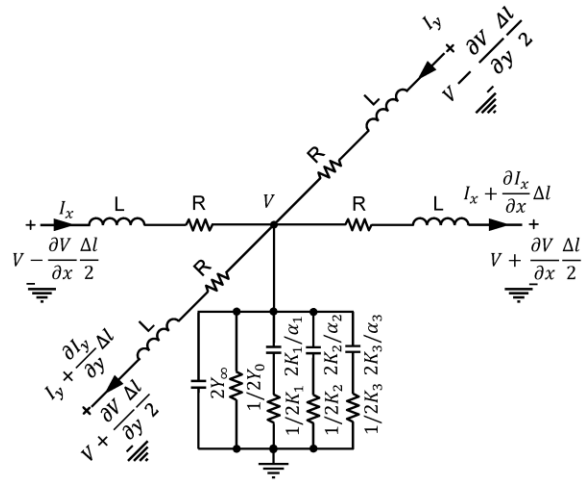

Fig. 3. 2D transmission line model based on Debye parametric model.

Table 5: Equivalence between parameters of transmission line in Fig. 3 versus Debye parameters

TLM Parameters		EM Field/Debye Parameters
L (H/m)	$\leftrightarrow$	μ (kgm/s^2/A^2)
$2Y_\infty$ (F/m)	$\leftrightarrow$	$\varepsilon_\infty\varepsilon_0$ (s^{4}A^2/kg/m^3)
$2Y_0$ (1/Ω/m)	$\leftrightarrow$	σ_s (1/Ω/m)
$2K_1$ (1/Ω/m)	$\leftrightarrow$	$\frac{\varepsilon_0\Delta\varepsilon_1}{\tau_1}$ (s^{3}A^2/kg/m^3)
$2K_2$ (1/Ω/m)	$\leftrightarrow$	$\frac{\varepsilon_0\Delta\varepsilon_2}{\tau_2}$ (s^{3}A^2/kg/m^3)
$2K_3$ (1/Ω/m)	$\leftrightarrow$	$\frac{\varepsilon_0\Delta\varepsilon_3}{\tau_3}$ (s^{3}A^2/kg/m^3)
α_1 (1/Ω/F)	$\leftrightarrow$	$\frac{1}{\tau_1}$ (1/s)
α_2 (1/Ω/F)	$\leftrightarrow$	$\frac{1}{\tau_2}$ (1/s)
α_3 (1/Ω/F)	$\leftrightarrow$	$\frac{1}{\tau_3}$ (1/s)

Although the computational complexity of Debye parametric model is lower, its biggest drawback is it cannot describe complex permittivity of a medium very accurately [36]. In their study, Salahuddin et al. [37], Debye parametric model is optimized for 500MHz and 20GHz frequency range to reduce the error introduced by the model.

Debye parameters given in [37] is used for analysing EM distribution in the human eye problem for 700MHz and 42GHz frequency range. However, some of the frequencies of interest in this study are out of the frequency range given in [37]. Maximum deviation error is for the conductivities of the tissues is about 7% and for the relative permittivity is about 3%. This will introduce a computational error. However, it can be said that the error is negligible since the electric field magnitude at these higher frequencies of interest, as it can be seen in Fig. 8, is almost zero. The Debye parameters for the ocular tissues are given in Table 6.

Table 6: Debye parameter values of the ocular tissues [37]

Tissue	ε_∞	σ_s	$\Delta\varepsilon_1$	$\Delta\varepsilon_2$	$\Delta\varepsilon_3$	τ_1 [ps]	τ_2 [ps]	τ_3 [ps]
a	8	1	100	48.4	11.2	674.8	7.111	20.94
c	8.3	0.8	39.2	62.1	6.5	8.066	1200	40.11
i	8.8	0.7	4.93	41	11.6	40.11	7.549	769.1
l	6.3	0.6	2.4	8.3	30.1	153.1	19.27	6.822
s	8	0.9	39.7	4	6.5	7.73	260.1	29.49
v	6.5	1	100	57.6	5.4	1259	7.362	21.71

*a: aqueous humor, c: cornea, i: iris, l: lens, s: sclera, v: vitreous humor.

B. TLM for bioheat transfer

Bioheat transfer in the human eye is calculated with Klinger's model, a continuum model of Pennes' model, in which the effect of non-unidirectional blood flow is taken into consideration [38]. It can also model noncompressible fluid flow in the tissues such as the flow in aqueous humor. Klinger's model can be described as:

$$\rho_T C_T \frac{\partial T}{\partial t} + (\rho_T C_T)\vec{u}.\nabla T = k_T \nabla^2 T + \omega_b C_b (T_b - T) + Q. \quad (18)$$

Where ρ_T is density of tissue (kg/m^3), C_T specific heat capacity of tissue $(Ws/kg/K)$, T is temperature (K), t is time (s), $\vec{u}$ is the velocity vector (m/s), k_T is thermal conductivity of tissue $(W/m/K)$, ω_b is blood perfusion rate $(kg/m^3/s)$, C_b is specific heat capacity of blood $(Ws/kg/K)$, T_b is the initial temperature value of blood (K) and Q is the sum of metabolic heat generation rate and the electromagnetic power density absorbed by the tissues (W/m^3). (18) can be rearranged as:

$$\nabla^2 T = \frac{\rho_T C_T}{k_T} \frac{\partial T}{\partial t} + \frac{(\rho_T C_T)}{k_T} \vec{u}\nabla T + \frac{\omega_b C_b}{k_T}(T - T_b) - \frac{Q}{k_T}. \quad (19)$$

Bioheat transfer problem can also be solved with TLM method [13, 39]. For this, transmission line model shown in Fig. 4 is used.

In the literature, the studies on solving bioheat transfer problems with TLM method often ignore the effects of noncompressible fluid flow in the tissues. In some cases, this may lead to small spatial errors on the distribution of temperature at tissues. To cope with this drawback, transmission line model for solving bioheat transfer problems is modified by adding dependent voltage sources as shown in Fig. 4. Hence, the modified transmission line model can reduce the spatial temperature distribution errors.

If the circuit analysis for the circuit shown Fig. 4 is performed as in the previous section, the following equation is obtained:

$$\nabla^2 V = 2LC \frac{\partial^2 V}{\partial t^2} + 2(LG + RC)\frac{\partial V}{\partial t} + 2RGV$$
$$+ \frac{2a_x}{\Delta l}\frac{\partial V}{\partial x} + \frac{2a_y}{\Delta l}\frac{\partial V}{\partial y} - \frac{L}{\Delta l}\frac{\partial I_s}{\partial t} - \frac{I_s R}{\Delta l}. \quad (20)$$

Here R, L, C and G are resistance, inductance, capacitance and conductance per meter of the transmission line respectively, Δl is the unit length of the transmission line in the both x and y axis, and the value a_x and a_y are the gain of the voltage controlled voltage sources. If the value of L is taken as 0 (or $\omega L \ll R$) the following is obtained:

$$\nabla^2 V = 2RC \frac{\partial V}{\partial t} + 2RGV + \frac{2a_x}{\Delta l}\frac{\partial V}{\partial x} + \frac{2a_y}{\Delta l}\frac{\partial V}{\partial y} - \frac{I_s R}{\Delta l}. \quad (21)$$
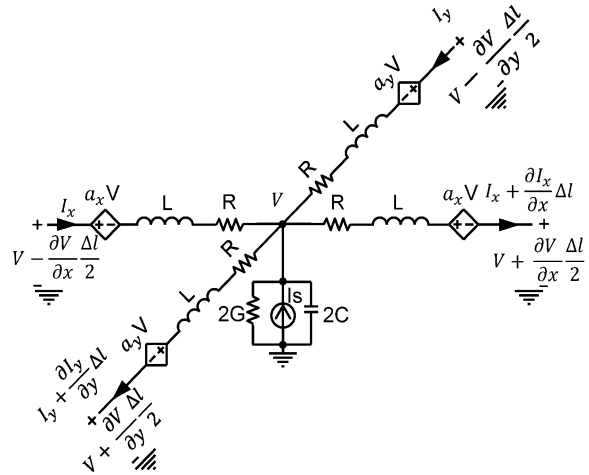

Fig. 4. Transmission line model for bioheat transfer.

As it can be seen in (19) and (21) that their solutions are mathematically equivalent with:

$$V \leftrightarrow T, \ 2RC \leftrightarrow \frac{\rho_T C_T}{k_T}, \ 2RG \leftrightarrow \frac{\omega_b C_b}{k_T},$$
$$\frac{2a_x}{\Delta l} \leftrightarrow \frac{\rho_T C_T}{k_T}u_x, \ \frac{2a_y}{\Delta l} \leftrightarrow \frac{\rho_T C_T}{k_T}u_y, \ \frac{I_s R}{\Delta l} \leftrightarrow \frac{\omega_b C_b T_b + Q}{k_T}. \quad (22)$$

The value of lumped elements and sources in Fig. 4 can be calculated as:

$$C \leftrightarrow \rho_T C_T \Delta l, a_x \leftrightarrow \frac{C_T}{4k_T}\omega_b \Delta l^2, a_y \leftrightarrow \frac{C_T}{4k_T}\omega_b \Delta l^2,$$

$$R \leftrightarrow \frac{1}{2k_T \Delta l}, G \leftrightarrow \omega_b C_b \Delta l, I_s \leftrightarrow 2(\omega_b C_b T_b + Q)\Delta l^2. \quad (23)$$

Thermal properties of the tissues are given in Table 7.

Table 7: Thermal properties of the tissues [30]

Tissue	ρ_T	C_T	k_T	Q_{met}	ω_b
a	993.8	3997	0.58	-	-
c	1062	3615	0.54		-
i	1091	3421	0.50	43899	32.3
l	1076	3133	0.43	-	-
s	1032	4200	0.58	6073	6.74
v	1005	4047	0.59	-	-

*a: aqueous humor, c: cornea, i: iris, l: lens, s: sclera, v: vitreous humor.

III. SIMULATION AND RESULTS

Simulations are performed for a far field radiation and the power density of the incoming electric field is assumed as the top of the general public exposure limit of ICNIRP (International Commission on Non-Ionizing Radiation Protection) guideline. The limits are given in Table 8 for the 5G frequencies used in the study.

Table 8: Reference level for general public exposure of EM field [40]

Frequency (GHz)	E Field RMS Strength (V/m)	Plane Wave Power Density (mW/cm²)
0.7	36	0.35
3.6	61	1
26	61	1
32	61	1
42	61	1

In the TLM based simulation, the proposed transmission line model based on three-term Debye parameters is used. In the TLM simulation, all the electric field distribution results obtained with a single simulation run for the frequencies of interest. Moreover, the lumped element values of the proposed transmission line are calculated from Debye parameters given in Table 6 in accordance with the equivalence given in Table 5. On the other hand, FEM based simulations are carried out by the number the frequencies of interest, even though FEM based simulation supports the parametric model of the tissues. The reason for this is that the FEM based simulations are carried out for comparison and in these simulations dielectric properties of the tissues given in [30] are used.

The simulation setup is shown in Fig. 5. In both EM and bioheat transfer problems, a square TLM mesh is used. The size of the mesh is 0.3mm X 0.3mm. A 2D TLM consists of two transmission line in each direction. Hence, the spatial resolution in each direction is the half of the side length of the square mesh. Since a 2D TLM

shunt node is used in the problems, the spatial resolution is 0.15mm and this resolution value is less than a tenth of wavelengths given in Tables 2 and 3, hence, it can be said that the spatial resolution is much lesser than wavelength in all EM and bioheat transfer problems.

In the simulation setup, cornea has a boundary with air medium while sclera has a boundary with head. The rest of the air and head medium in Fig. 5 are truncated with matched boundary condition as described in [29] for the electric field distribution calculation. The impedance connected at the matched boundary is chosen to be equal to the characteristic impedance of the medium. The region labelled as air in Fig. 5 is truncated with impedance that equals to the characteristic impedance of air and the region labelled as head in Fig. 5 is truncated with impedance that equals to the characteristic impedance of head tissue. The dielectric properties of the head tissue are taken as the average of that of white and gray matter as in [41].
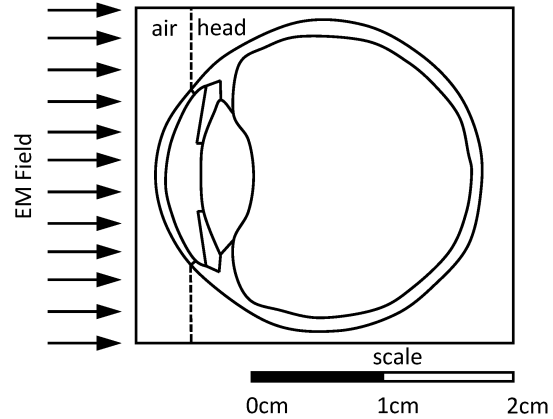

Fig. 5. Simulation setup.

Since the field considered to be come at right angles, the matched boundary condition will give good results with low computational complexity [29]. The circuit representation of matched boundary condition is given in Fig. 6.
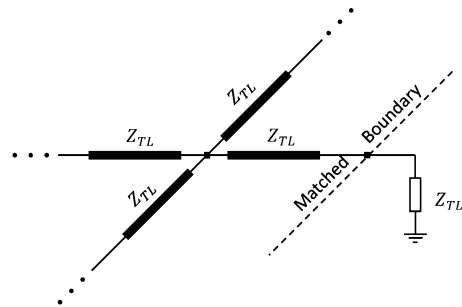

Fig. 6. Circuit representation of matched boundary condition.

The reflection coefficient at the boundary is calculated as follows:

$$\Gamma = \frac{Z_{Load} - Z_{TL}}{Z_{Load} + Z_{TL}} = \frac{Z_{TL} - Z_{TL}}{Z_{TL} + Z_{TL}} = 0. \qquad (24)$$

For bioheat transfer problem convection boundary condition is used. The convection boundary condition is described as:

$$-k_T \frac{\partial T}{\partial l} = h(T - T_T). \qquad (25)$$

Here h $(W/m^2/K)$ is the heat transfer coefficient between two region and T_T (K) is the temperature at the boundary. In Fig. 7, the resistance R is used to model the heat transfer coefficient and the voltage source V_T is used to model the temperature at the boundary and their relations can be found in [42] and are given in (26):

$$h \leftrightarrow \frac{1}{2R\Delta l}, T_{T \leftrightarrow} V_T. \qquad (26)$$

Convection boundary is considered for two different boundaries. First one is the boundary between air and cornea and the second one is between sclera and head regions. The heat transfer coefficients for these boundaries are taken as in [43]. Also, the ambient temperature is taken as 25℃ and the body temperature is taken as 37℃. The convection boundary in TLM is used as described in [42] and shown in Fig. 7.
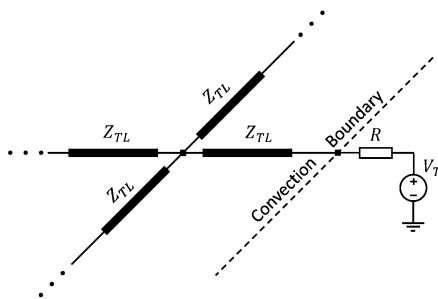

Fig. 7. Circuit representation of convection boundary condition.

The electric field distribution in the human eye is calculated with both TLM and FEM methods and their results are given in Fig. 8. As it can be seen in the figure, both results of TLM and FEM based electric field distribution calculation are close to each other.

As it can be seen in Fig. 8, at the lowest frequency, the electric field magnitude gradually decreasing as it travels inside the human eye, but it never reaches down to zero. For 3.6GHz frequency, the electric field magnitude inside human eye exceeds that of incoming field and the maxima occurs at a region between aqueous humour and lens tissues. Electric field distribution at the higher frequencies (26, 32 and 42GHz) can only be observed at near the cornea and at the other part of the eye electric field magnitude is almost zero.
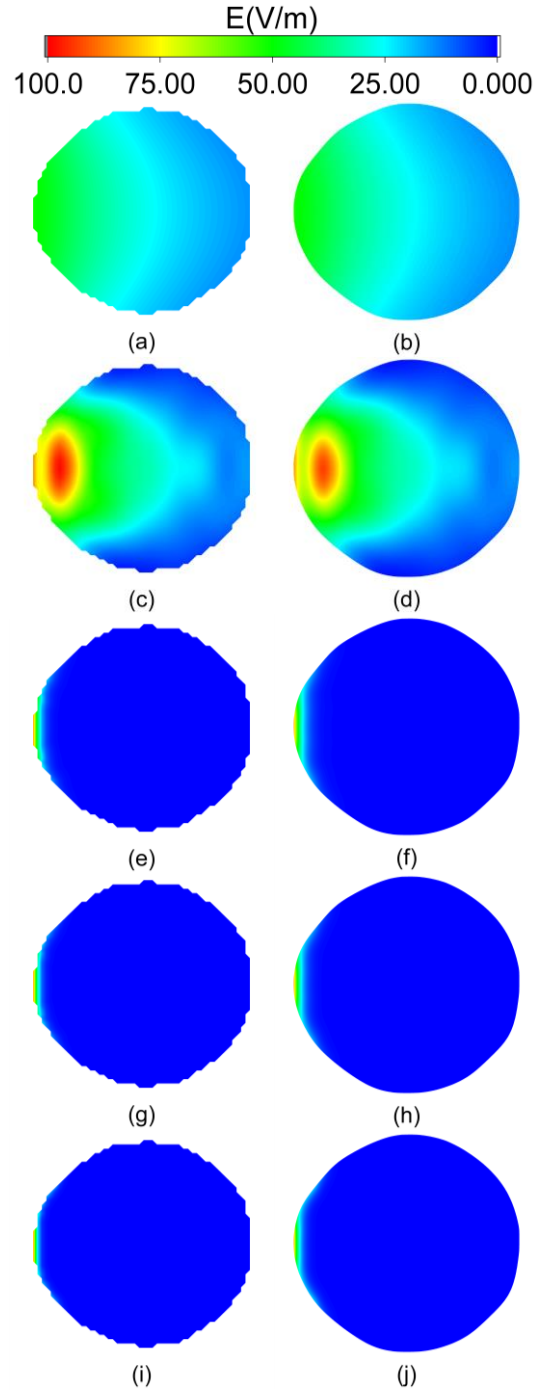

Fig. 8. Electric field distributions inside of the human eye at 700MHz ((a) TLM - (b) FEM), 3.6GHz ((c) TLM - (d) FEM), 26GHz ((e) TLM - (f) FEM), 32 GHz ((g) TLM - (h) FEM) and 42 GHz ((i) TLM - (j) FEM).

Specific absorption rate (SAR) values of the ocular tissues for the frequencies of interest are calculated before calculation of temperature distribution in the human eye. SAR calculated by using (27):

$$SAR = \frac{\sigma E_{rms}^2}{\rho}.\qquad(27)$$

Here σ is the conductivity of tissue and ρ is the density of tissue. The SAR in the human eye is calculated by using electric field distributions obtained from TLM and FEM based calculations and given in Fig. 9 for both methods. At the lower frequencies (700MHz and 3.6GHz) maximum SAR value is observed at aqueous humor due to its higher conductivity. On the other hand, at the higher frequencies (26GHz, 32GHz and 42GHz) maximum SAR value observed at cornea for at these frequencies maximum of the electric field magnitudes are observed at the surface.
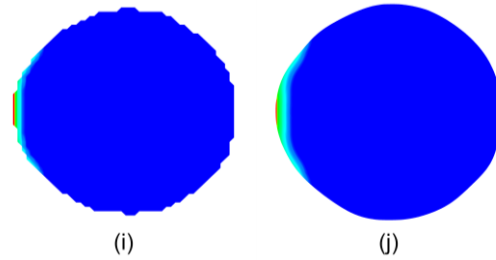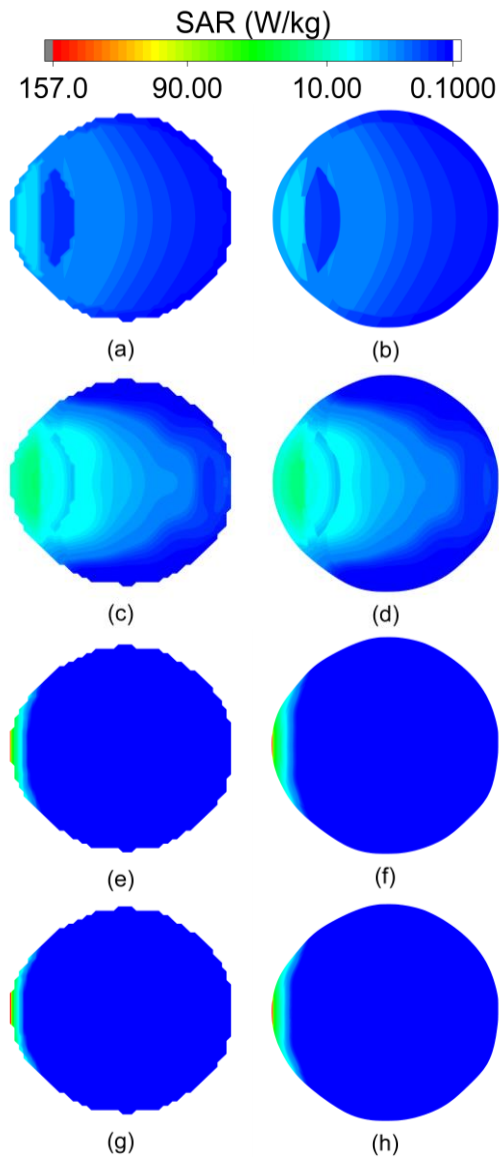

(i)   (j)

Fig. 9. SAR distributions inside of the human eye at 700MHz ((a) TLM - (b) FEM), 3.6GHz ((c) TLM - (d) FEM), 26GHz ((e) TLM - (f) FEM), 32 GHz ((g) TLM - (h) FEM) and 42 GHz ((i) TLM - (j) FEM).

SAR (W/kg)

157.0   90.00   10.00   0.1000

(a)   (b)

(c)   (d)

(e)   (f)

(g)   (h)

The temperature distribution in the human eye is also calculated with TLM method for two different cases. In the first one, the effects of fluid dynamics in aqueous humor are not considered while in the second one these effects are considered. As in the electric field distribution calculation, FEM based calculation of the temperature distribution in the human eye is also carried out for comparison. In the simulation, exposure time is assumed as 30 minutes. Also, the subject of the experiment is considered as in standing position.

The temperature rise due to exposure to EM field at 5G frequencies are given in Fig. 10 for the case where fluid flow in aqueous humor is neglected. As it can be seen in the figure the results of TLM, and FEM based calculations are very close to each other.

For the second case where the effects of fluid flow in aqueous humor are considered, the temperature rise due to exposure to EM field at 5G frequencies are given in Fig. 11. As in the previous case, the results of TLM and FEM based calculations are very close to each other.

As seen in Figs. 10 and 11, the highest temperature rise occurs at 3.6GHz and the lowest one occurs at 700MHz. For the rest of the frequencies the temperature rise decreases as the frequency increases. There are two main reason for why the lowest temperature rise occurs at 700MHz. The first one is the power density is at 700MHz is lower than at other frequencies and the second one is at 700MHz tissue conductivities are the lowest. The highest rise is observed at 3.6GHz since the magnitude of electric field distribution is the highest at this frequency.

When both Figs. 10 and 11 are examined, there is a little difference between both figures in terms of temperature rise distributions. The difference can be easily observed at aqueous humor and its neighbour regions. However, the maximum temperature rises in both case at all frequencies is very close to each other.
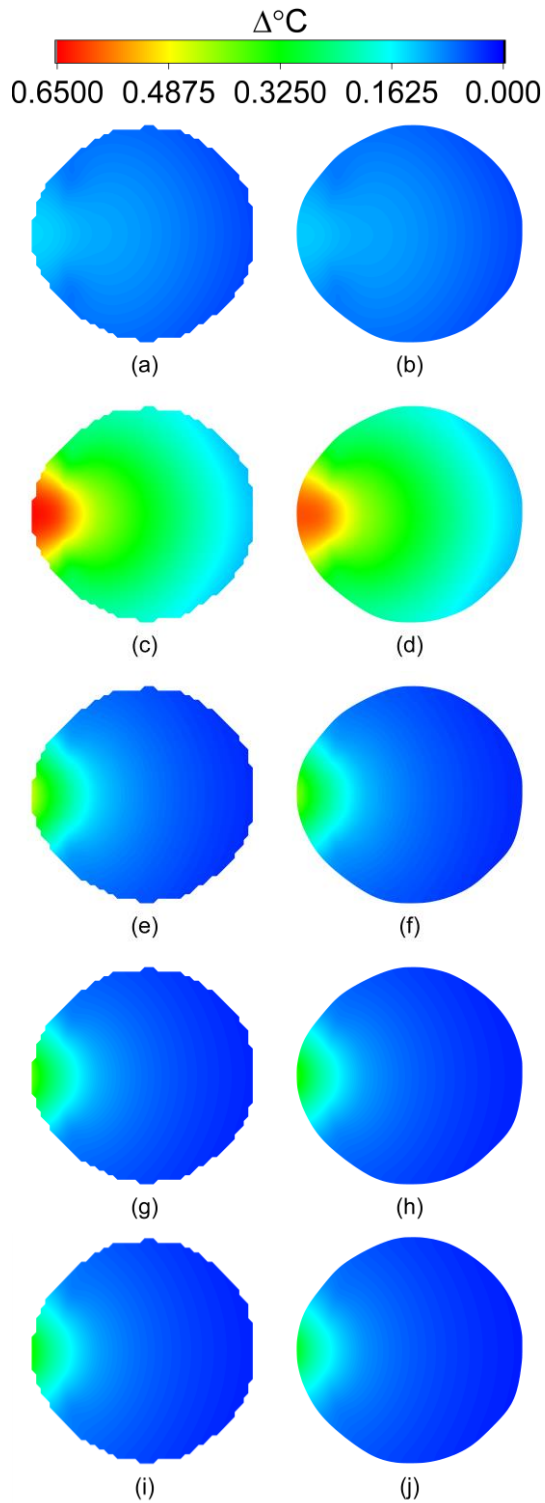
Fig. 10. Temperature rise distribution in the human eye when the aqueous humor flow dynamics are neglected, after 30 minutes exposure to EM fields at 700MHz ((a) TLM - (b) FEM), 3.6GHz ((c) TLM - (d) FEM), 26GHz ((e) TLM - (f) FEM), 32 GHz ((g) TLM - (h) FEM) and 42 GHz ((i) TLM - (j) FEM).
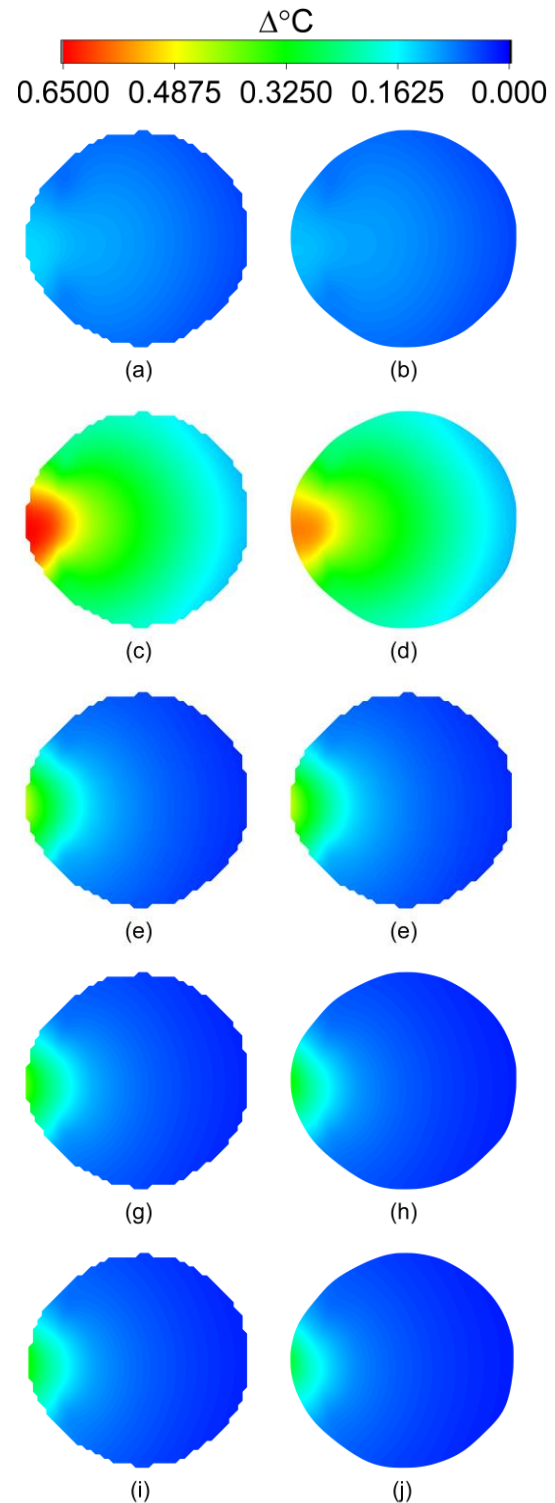
Fig. 11. Temperature rise distribution in the human eye when the aqueous humor flow dynamics are considered, after 30 minutes exposure to EM fields at 700MHz ((a) TLM - (b) FEM), 3.6GHz ((c) TLM - (d) FEM), 26GHz ((e) TLM - (f) FEM), 32 GHz ((g) TLM - (h) FEM) and 42 GHz ((i) TLM - (j) FEM).

Since the effect of the aqueous humor (AH) flow dynamics on temperature rise distribution is not very apparent from Figs. 10 and 11, temperature rise distributions in the neighbourhood of aqueous humor at 3.6 GHz for both FEM and TLM methods are given in Fig. 12.
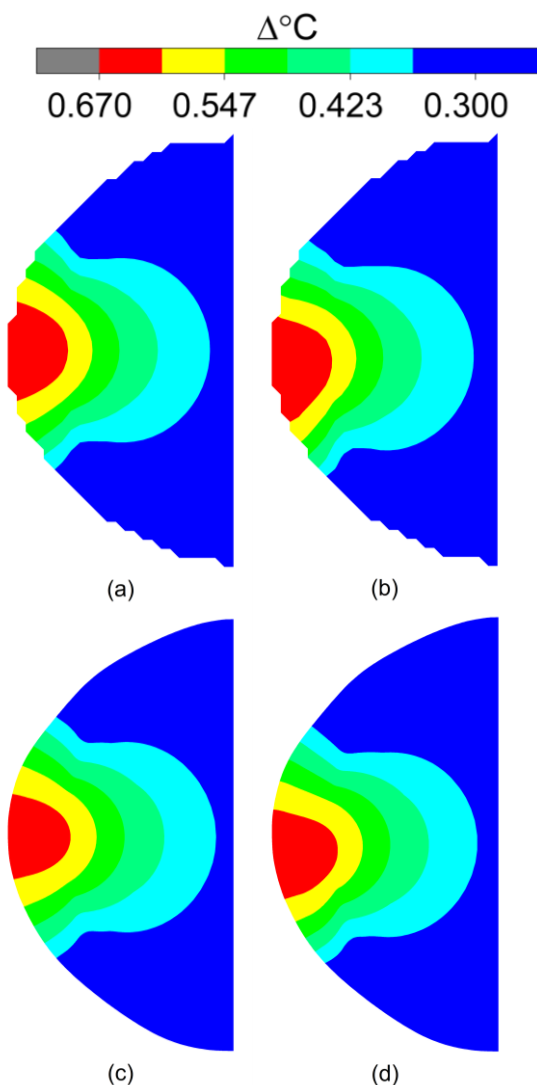

Fig. 12. Temperature rise distribution in the human eye after 30 minutes exposure to EM fields at 3.6 GHz (a) TLM without AH flow, (b) TLM with AH flow, (c) FEM without AH flow, and (d) FEM with AH flow.

IV. CONCLUSION

In this work, calculation of electric field distribution in human eye and temperature rise due to exposure to electric field is carried with TLM method. Temperature increase is calculated with Klinger's bioheat transfer equation for 30 minutes exposure for a standing person. Moreover, both electric field distribution and its resultant temperature increase in human eye is calculated

with FEM method. The all results of TLM based calculations are consistent with that of FEM based calculations.

From temperature rise point of view, Bernardi et al. [4] defined the temperature rise limits as 0.3℃ for lens and 1℃ for cornea tissue. These temperature limits are a tenth of the temperatures at which thermal damage (cataract) to the eye can occur. For all the frequencies this limit is not exceeded in both cases except at 3.6GHz. At this frequency the maximum temperature rise on the cornea is 0.65℃, which is below the limit, while the maximum temperature rise at the lens is around 0.5℃ that its thermal effect may not be neglected and is needed to be investigated further.

REFERENCES

[1] A. Gupta and R. K. Jha, "A survey of 5G network: Architecture and emerging technologies," *IEEE Access*, vol. 3, pp. 1206-1232, July 2015.

[2] P. K. Agyapong, M. Iwamura, D. Staehle, W. Kiess, and A. Benjebbour, "Design considerations for a 5G network architecture," *IEEE Communications Magazine*, vol. 52, no. 11, pp. 65-75, Nov. 2014.

[3] Y. Diao, S. Leung, Y. He, W. Sun, K. Chan, Y. Siu, and R. Kong, "Detailed modelling of palpebral fissure and its influence on SAR and temperature rise in human eye under GHz exposures," *Bio-electromagnetics*, vol. 37, pp. 256-263, Apr. 2016.

[4] P. Bernardi, M. Cavagnaro, S. Pisa, and E. Piuzzi, "SAR distribution and temperature increase in an anatomical model of the human eye exposed to the field radiated by the user antenna in a wireless LAN," *IEEE Transactions on Microwave Theory and Techniques*, vol. 46, no. 12, pp. 2074-2082, Dec. 1998.

[5] A. Hirata, S. Matsuyama, and T. Shiozawa, "Temperature rises in the human eye exposed to EM waves in the frequency range 0.6-6 GHz," *IEEE Transactions on Electromagnetic Compatibility*, vol. 42, no. 4, pp. 386-393, Nov. 2000.

[6] T. Wessapan and P. Rattanadecho, "Specific absorption rate and temperature increase in human eye subjected to electromagnetic fields at 900 MHz," *ASME Journal of Heat Transfer*, vol. 134, no.9, pp. 091101-01-091101-11, July 2012.

[7] Y. Diao, S. Leung, K. H. Chan, W. Sun, Y.-M. Siu, and R. Kong, "The effect of gaze angle on the evaluations of SAR and temperature rise in human eye under plane-wave exposures from 0.9 to 10 GHz," *Radiation Protection Dosimetry*, vol. 172, no. 4, pp. 393-400, Dec. 2016.

[8] T. Wessapan, P. Rattanadecho, and P. Wongchadakul, "Effect of the body position on natural convection within the anterior chamber of the human eye during exposure to electromagnetic fields," *Numerical Heat Transfer, Part A:*

Applications, vol. 69, no. 9, pp. 1014-1028, Jan. 2016.

[9] S. Otsu, T. Michiyama, and S. Kuwano, "Body effect on SAR in the human eye close to metallic spectacles for plane-microwave exposure," *IEICE Communications Express*, vol. 6, no. 10, pp. 602-606, 2017.

[10] S. Kuwano, M. Kobayashi, and T. Michiyama, "SAR analysis in the eye of human whole-body model for plane-microwave exposure," *IEICE Communications Express*, vol. 6, no. 4 pp. 172-176, 2017.

[11] J. Lan, T. Hong, X. Liang, and G. Du, "Evaluation of microwave microdosimetry for human eyes with glasses exposed to wireless eyewear devices at phone call state," *Progress in Electromagnetics Research M*, vol. 63, pp. 71-81, 2018.

[12] N. Cvetković, D. Krstić, V. Stanković, and D. Jovanović, "Electric field distribution and SAR inside a human eye exposed to VR glasses," *IET Microwaves, Antennas & Propagation*, vol. 12, no. 14, pp. 2234-2240, Nov. 2018.

[13] H. F. Milan and K. G. Gebremedhin, "General node for transmission-line modeling (TLM) method applied to bio-heat transfer," *International Journal of Numerical Modelling: Electronic Networks, Devices and Fields*, vol. 31 no. 5, May 2018.

[14] A. Karampatzakis and S. Theodoros, "Numerical model of heat transfer in the human eye with consideration of fluid dynamics of the aqueous humour," *Physics in Medicine & Biology*, vol. 55, no. 19, pp. 5653-5665, Oct. 2010.

[15] Report B from CEPT to the European Commission in response to the Mandate "to develop harmonised technical conditions for spectrum use in support of the introduction of next-generation (5G) terrestrial wireless systems in the union," Harmonised technical conditions for the 24.25-27.5 GHz ('26 GHz') frequency band, 2018.

[16] P. P. Silvester and R. L. Ferrari, *Finite Elements for Electrical Engineers*, Cambridge University Press, Cambridge, UK, 1996.

[17] J. Liu, Z. Ren, and C. Wang, "Interpretations of living tissue's temperature oscillations by thermal wave theory," *China Science Bulletin*, vol. 40, pp. 1493-1495, 1995.

[18] J. Liu, X. Zhang, C. Wang, W.Q. Lu, and Z. Ren, "Generalized time delay bioheat equations and preliminary analysis on its wave nature," *China Science Bulletin*, vol. 42, pp. 289-292, Feb. 1997.

[19] S. Ozen, S. Helhel, and O. Cerezci, "Heat analysis of biological tissue exposed to microwave by using thermal wave model of bio-heat transfer (TWMBT)," *Burns: Journal of the International Society for Burn Injuries*, vol. 34, no. 1, pp. 45-49, Jan. 2008.

[20] W. Kaminski, "Hyperbolic heat conduction equation for materials with a nonhomogeneous inner structure," *ASME Journal of Heat Transfer-Transactions*, vol. 112, pp. 555-560, Aug. 1990.

[21] K. Mitra, S. Kumar, A. Vedavarz, and M. K. Moallemin, "Experimental evidence of hyperbolic heat conduction in processed meat," *ASME Journal of Heat Transfer-Transactions*, vol. 117, pp. 568-573, Aug. 1995.

[22] W. Roetzel, N. Putra, and S. K. Das, "Experiment and analysis for non-Fourier conduction in materials with non-homogeneous inner structure," *International Journal of Thermal Sciences*, vol. 42, pp. 541-552, Oct. 2003.

[23] Y. Zhang, "Generalized dual-phase lag bioheat equations based on non-equilibrium heat transfer in living biological tissues," *International Journal of Heat Mass Transfer*, vol. 52, pp. 4829-4834, Feb. 2009.

[24] S. C. DeMarco, G. Lazzi, W. Liu, J. D. Weil, and M. S. Humayun, "Computed SAR and thermal elevation in a 0.25-mm 2-D model of the human eye and head in response to an implanted retinal stimulator-Part I: Models and methods," *IEEE Transactions on Antennas and Propagation*, vol. 51, no. 9, pp. 2274-2285, Sep. 2003.

[25] T. Wessapan and P. Rattanadecho, "Aqueous humor natural convection of the human eye induced by electromagnetic fields: In the supine position," *Journal of Medical and Bioengineering*, vol. 3, no. 4, Dec. 2014.

[26] K. Wakino, T. Nishikawa, and Y. Ishikawa, "Miniaturization technologies of dielectric resonator filters for mobile communications," *IEEE Transactions on Microwave Theory and Techniques*, vol. 42, no. 7, pp. 1295-1300, July 1994.

[27] M. Höft and M. Thore, "Compact base-station filters using TM-mode dielectric resonators," *German Microwave Conference GeMIC, Karlsrhue*, Mar. 2006.

[28] M. Mantash, A. Kesavan, and T. A. Denidni, "Beam-tilting endfire antenna using a single-layer FSS for 5G communication networks," *IEEE Antennas and Wireless Propagation Letters*, vol. 17, no. 1, pp. 29-33, Nov. 2018.

[29] C. Christopoulos and C. Christopoulos, *The Transmission-line Modeling Method: TLM*, IEEE Press, New York, USA, 1995.

[30] IT'IS Foundation tissue properties database, https://itis.swiss/virtual-population/tissue-properties/database/database-summary/, Accessed on Jan. 21, 2019.

[31] H. P. Schwan and K. R. Foster, "RF-field interactions with biological systems: Electrical properties and biophysical mechanisms," *Proceedings of the IEEE*, vol. 68, no. 1, pp. 104-113, Jan. 1980.

[32] M. A. Stuchly, "Biological effects of electromagnetic

fields," *International Journal of Bioelectromagnetism*, vol. 4 no. 2, pp. 157-160, 2002.

[33] M. A. Eleiwa and A. Z. Elsherbeni, "Debye constants for biological tissues from 30 Hz to 20 GHz," *Applied Computational Electromagnetics Society Journal*, vol. 18, no. 3, pp. 202-213, Nov. 2001

[34] F. Kaburcuk and A. Z. Elsherbeni, "Temperature rise and SAR distribution at wide range of frequencies in a human head due to an antenna radiation," *Applied Computational Electromagnetics Society Journal*, vol. 33, no. 4, pp. 367-372, Apr. 2018.

[35] F. Kaburcuk and A. Z. Elsherbeni, "Efficient computation of SAR and temperature rise distributions in a human head at wide range of frequencies due to 5G RF field exposure," *Applied Computational Electromagnetics Society Journal*, vol. 33, no. 11, pp. 367-372, Nov. 2018.

[36] K. S. Cole and R. H. Cole, "Dispersion and absorption in dielectrics I. Alternating current characteristics," *The Journal of Chemical Physics*, vol. 9, no. 4, pp. 341-351, 1941.

[37] S. Salahuddin, E. Porter, F. Krewer, and M. O'Halloran, "Optimised analytical models of the dielectric properties of biological tissue," *Medical Engineering &Pphysics*, vol. 43, pp. 103-111, Mar. 2017.

[38] H. G. Klinger, "Heat transfer in perfused biological tissue—I: General theory," *Bulletin of Mathematical Biology*, vol. 36, no. 4, pp. 403-415, June 1974.

[39] A. A. Ijjeh and M. Ney, "Local time-step TLM unstructured block meshing for electromagnetic and bio-thermal applications," *IEEE Journal on Multiscale and Multiphysics Computational Techniques*, vol. 2, pp. 174-182, Nov. 2017.

[40] A. Ahlbom, U. Bergqvist, J. H. Bernhardt, J. P. Cesarini, M. Grandolfo, M. Hietanen, A. F. Mckinlay, M. H. Repacholi, D. H. Sliney, J. A. Stolwijk, and M. L. Swicord, "Guidelines for limiting exposure to time-varying electric, magnetic, and electromagnetic fields (up to 300 GHz)," *Health Physics*, vol. 74, no. 4, pp. 494-521, 1998.

[41] M. Cvetkovič, S. Lallechere, K. E. Khamlichi Drissi, P. Bonnet, and D. Poljak, "Stochastic sensitivity in homogeneous electromagnetic-thermal dosimetry model of human brain," *Applied Computational Electromagnetics Society*, vol. 31, no. 6, June 2016.

[42] H. F. Milan and K. G. Gebremedhin, *Journal of Thermal Biology*, vol. 62, pp. 116-122, Feb. 2016.

[43] E. H. Ooi and W. T. Ang, "A boundary element model of the human eye undergoing laser thermo-keratoplasty," *Computers in Biology and Medicine*, vol. 38, no. 6, pp. 727-737, July 2008.

Burak Aricioglu was born in 1989. He received B.Sc. and M.Sc. degrees in Electrical and Electronics Engineering from Bogazici University in 2011 and 2014, respectively and Ph.D. degree in Electrical & Electronics Engineering from Sakarya University in 2019. He is, currently, a Research Assistant at Sakarya University of Applied Sciences. His main research interests are nonlinear systems analysis, and bioelectromagnetic interactions.

Abdullah Ferikoglu was born in 1953, received his B.Sc. in Electronics and Communications Engineering from Istanbul Technical University in 1982, his M.S. degree in Electronics and Computer Education from Marmara University in 1992 and Ph.D. degree in Electronics and Communications Engineering department from Istanbul Technical University in 1996. He is now with Sakarya University of Applied Sciences, Electrical and Electronics Engineering Department. His research areas include circuit analysis and design, modeling and simulation, and biomedical engineering.